Influence of droplet velocity, spacing, and inter-arrival time on line formation and saturation in binder jet additive manufacturing

By: Trenton Colton, Nathan B. Crane

Department of Mechanical Engineering, Brigham Young University, Provo, Utah

**Corresponding Author, nbcrane@byu.edu*

ABSTRACT

Binder Jetting (BJ) is a low-cost Additive Manufacturing (AM) process that uses inkjet technology to selectively bind particles in a powder bed. BJ relies on the ability to control, not only the placement of binder on the surface but also its imbibition into the powder bed. This is a complex process in which picoliter-sized droplets impact powder beds at velocities of 1-10 m/s. However, the effects of printing parameters such as droplet velocity, size, spacing, and inter-arrival time on saturation level (fraction of pore space filled with binder) and line formation (merging of droplets to form a line) are unknown. Prior attempts to predict saturation levels with simple measurements of droplet primitives and capillary pressure assume that droplet/powder interactions are dominated by static equilibrium and neglect the impact of printing parameters. This study analyzes the influence of these parameters on the effective saturation level and conditions for line formation when printing single lines into powder beds of varied materials (316 stainless steel, 420 stainless steel, and alumina) and varied particle size (d_{50} = 10-47 microns). Results show that increasing droplet velocity or droplet spacing decreases effective saturation while droplet spacing, velocity, and inter-arrival time affect line formation. At constant printing velocity, the conditions for successful line printing are shown to be a function of droplet spacing and square root of the droplet inter-arrival time analogous to the Washburn model for infiltration into a porous media. The results have implications to maximizing build rates and improving quality of small features in BJ.

KEYWORDS

Inkjet, Binder Jetting, saturation, balling, additive manufacturing, Washburn infiltration

INTRODUCTION

Binder Jetting (BJ) is a low-cost additive manufacturing (AM) process that combines a powder bed with inkjet printing technology. In this process, powder is spread in thin layers and an inkjet print head deposits droplets to bind powder in the region of the desired cross-section. A new layer of powder is spread on top, and this process is repeated layer-by-layer [1]. A drying or heating process is often included between layers. BJ uses powder from lower layers as a support for upper layers. The lack of large thermal heating to cause a phase change and the use of inkjet technology enables faster printing speeds than most competing technologies. The resulting "green" part can be post-processed by sintering or infiltration to improve part properties such as strength and density [1, 2]. A major advantage of BJ over other AM processes is its ability to utilize almost any powdered material including polymers [3], ceramics [4] and metals [5]. Interest has grown as techniques for sintering homogenous materials to full density have been refined [6-9].

As early BJ patents expire and overall AM demand grows, interest in BJ has increased. However, further BJ implementation in industry depends on improving dimensional accuracy, mechanical properties, and cost effectiveness. Much of the current research in BJ focuses on developing printing parameters for specific machines and specific materials [10-14]. However, an increased understanding of the physics of the binder/powder interaction will help researchers identify materials and corresponding print parameters independent of machine type and with reduced testing. Current modeling practices disregard the influence of printing parameters such as droplet velocity, droplet inter-arrival time, and heating/drying even though these parameters have shown to affect printing in BJ or related fields [15-19]. Improved understanding of these print parameters in BJ will allow for improved dimensional tolerances, enhanced material properties, and reduced minimum feature size, as well as decreased cost to develop new machines and material systems.

While BJ performance is affected by many factors including powder selection, printing parameters, and post processing, the key to BJ is the interaction of binder droplets with the powder bed to form a new region of bound powder. This agglomeration of powder bound by a single droplet (large or small) is referred to as a primitive. In BJ, many droplets are deposited in close proximity to form lines, layers, and 3D parts. Droplets 20-60 µm in diameter impact powder with velocities ranging from 1-10 m/s. The forces involved in the droplet/powder interaction are complex. Both capillary and inertial forces are significant and powder bed rearrangement is common [20]. While experiments have shown the impact of print parameters on part-level properties such as dimensional accuracy, porosity, and strength [21, 22], the impact of print parameters (droplet velocity, droplet size, droplet inter-arrival time, and droplet spacing) on the basic binder/powder interaction itself has not been reported.

During BJ, droplets impact the powder bed surface and begin to infiltrate into the pore space. Inertial forces dominate at short times while capillary pressure is the primary force acting on the fluid over longer time periods [27]. Capillary pressure varies with saturation and often has significant hysteresis (Figure 1). Binder will migrate through voids in powder bed until the pressure across the binder-air interface balances the wetting forces. Upon impact, droplets temporarily create fully saturated region on the surface—where the void space between powder

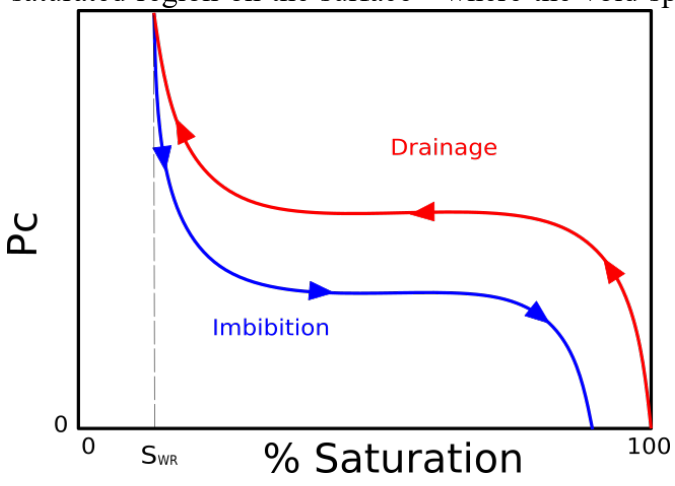

Figure 1: General trend of saturation for drainage and imbibition curves with capillary pressure (Pc). There is generally significant hysteresis between the imbibition and drainage curves. S_{WR} indicates the irreducible wetting saturation level. Adapted from [29].

particles is filled with binder. Surrounding unsaturated regions absorb binder as capillary pressure drives flow from saturated regions until equilibrium is reached. Due to powder packing variation and the hysteresis between the imbibition and drainage curves the saturation level can vary throughout the wetted region.

Miyanaji, et al. [28] proposed a physics-based model to predict the equilibrium saturation level from the measured capillary pressure based on a single equivalent pore size. It excluded the impact of in-process drying, droplet size, and droplet velocity. Unfortunately, the limited experimental data did not show consistent correlation between model predictions and part-level measurements [28]. Drying and droplet size have since been shown to have a significant impact on saturation levels [15].

Bai, et al. [30] explored saturation levels in primitives formed by millimeter-scale sessile drops. The study calculated the dynamic contact angle from measured imbibition times of sessile drops and attempted to correlate these measurements to saturation level [30]. It was found that as the dynamic contact angle increased the saturation level increased and binder penetration depth decreased.

Another printing parameter is saturation, the percentage of pore space filled by binder. Saturation is a function of the binder, powder (size, shape), packing fraction, and the distribution of pore sizes in the powder bed [31]. While saturation in BJ is typically taken as a single parameter, there is actually a range of equilibrium values due to hysteresis between the imbibition and drainage curves [31] (Figure 1). This range of potential values make it path dependent rather than a state variable. Thus, the effective saturation is likely to vary with the printing parameters. In this study, the binder/powder interaction is characterized in terms of a part's effective binder saturation (S_{eff}) by measuring the mass of powder bound by a known quantity of binder deposited using the equation:

$$S_{eff} = \frac{m_b \rho_{pb}}{m_p \rho_b * (1 - P_f)} \quad (1)$$

where m_b is the mass of the deposited binder, $\rho_b$is binder density, m_p is the mass of the bound powder, ρ_{pb} is powder bed density, and $P_f$is the packing fraction.

As droplets are printed adjacent to prior droplets, the bound regions merge into lines. The characteristics of line formation provide insight into the binder/powder interaction. Because nozzle pitch is larger than droplet diameters, most areas are formed by printing individual lines that are later joined. Line formation is particularly important to fine feature development. While minor defects in larger features may not be critical to part function, these defects in small features are critical to part structure. Understanding the formation of lines can help select printing parameters for improved speed or feature resolution.

Successful line formation is the ability to print uniform width lines without defects such as balling. Line formation as a measurement is used in 2D printing on solid surfaces [17, 18, 23, 24] but has been limited in application in 3D powder bed surfaces. Binder droplets seek a minimum energy state which can result in breakup into individual balls, bulges, or other defects in the line. While

[25] looked at the impact of printing frequency (droplet inter-arrival time) and spacing on line formation, the parameter range was too small to provide insight into the nature of the relationship.

Effective printing also requires the printed binder is sufficient to fully bind the powder within the part without spreading beyond it. A target print saturation is generally set by the user to determine how much binder is deposited per volume of the part. However, environmental conditions and interactions with previously printed regions can alter the quantity of bound powder per volume binder so that the effective saturation of the part may differ from the target saturation [15]. To continuously bind the powder together, the saturation must be sufficient to form a continuous network of fluid. If it is continuous, pressure is equilibrated throughout the network. As successive layers are deposited, hydrostatic pressure grows and may exceed capillary forces causing a defect commonly called “bleeding” in which the binder migrates beyond the desired part boundaries, decreasing dimensional and form accuracy [15, 26].

This paper focuses on the effects that varying key printing parameters in BJ (droplet velocity, size, spacing, and inter-arrival time) on line formation and effective saturation. Line formation can be a measurement of defects in BJ and assist in improving printing fine features. Effective saturation may differ from the target print saturation specified by the user. The difference may be due to inaccuracies in modeling by disregarding certain print parameters. Both line formation and saturation impact the accuracy and quality of printed parts. The relationships were analyzed by optical imaging and mass measurements of printed lines. These results are compared to single drop primitives from millimeter-scale droplets. This study builds upon previous work [32], with additional materials, a broader range of printing conditions, and an expanded analysis and discussion. The following section provide an overview of the effects of printing parameters on BJ-printed parts.

KEY PRINTING PARAMETERS

In BJ, individual droplets must coalesce within and between layers to form continuous features. However, fluids minimize their energy by forming spheres. BJ features successfully form when binder infiltrates into the powder before enough pools on the surface that surface energy minimization drives it to form bulges or pinch off into separate spheres (balling). The total quantity of binder deposited must also be controlled so that the effective saturation matches the printed saturation. Too little saturation weakens the green part while too high of saturation causes bleeding as binder moves beyond the printed regions. The line formation and saturation depend on print parameters.

The basic study of saturation and formation of a printed lines in a porous powder medium has received little attention. Most BJ studies focus on full parts while droplet studies utilize single millimeter-scale droplets. Interactions with adjacent droplets are known to have a significant impact but have not been evaluated [33]. Understanding the impact of printing parameters on effective saturation will guide future modeling on saturation. Line formation can lead to improved fine feature development. Understanding the impact of printing conditions on line formation and effective saturation will improve accuracy and quality of printed parts and reduce the time and

resources needed to evaluate new powders, binders, and machines. The key printing parameters are defined below.

Droplet Spacing and Size

BJ shares some principles in common with 2D inkjet printing on solid surfaces. For example, coalescence of individual droplets into lines of uniform width without bulges or necking is important to good 2D print quality. Line formation is known to depend on droplet size, droplet spacing, droplet velocity, and contact angle [17, 18, 23]. When printing on glass, smaller droplet spacing led to bulging while larger spacing did not coalesce to a single line [18]. While these 2D observations are helpful, relatively little is known about the conditions required for line formation in BJ. In BJ, droplet size, droplet spacing, and layer thickness determine the overlap between successive droplet primitives. Primitive overlap will result in increased green strength [22] but too much binder will decrease geometric accuracy [15]. Droplet overlap in powder also impacts build time and formation of defects such as balling [34].

Droplet Inter-arrival Time

The interaction between droplets and line formation on solid surfaces depends on droplet inter-arrival time [35]. Droplets deposited on a glass with a shorter inter-arrival period created a more uniform line than those printed at longer intervals [23]. However, the dynamics in BJ are more complex than 2D printing on solid surfaces as droplets can both spread over and penetrate into the pores between powder particles. In BJ, a short inter-arrival time is often detrimental to line formation [36]. Baker [25] using a continuous jet print head with large 90-100 μm droplets at frequencies of 6.7 to 40 kHz reported line formation and balling being connected to droplet spacing and inter-arrival time However, the reported frequencies were significantly higher and droplets much larger than characteristic of current BJ systems.

Droplet Velocity

Primitive formation also depends on droplet velocity at impact. Emady et al. [37] developed a map to identify conditions for granulation in millimeter scale droplets that delineates granule regimes with different vertical aspect ratios based on bond number and bed porosity. The regimes were correlated with impact velocity, powder size, powder shape, binder composition, and porosity [38, 39]. These studies, though insightful, use droplet sizes orders of magnitude larger than droplets in BJ. The studies also did not include effects of interaction with adjacent wetted powder which has been shown to significantly impact the wetting regimes [40]. In BJ, the interaction with adjacent moist regions is critical to creating 3D geometry from individual primitives.

Studies using in-situ high-speed optical and x-ray imaging have observed deformation of the powder bed during primitive formation [20, 36]. These studies visually show that the droplet transfers kinetic energy to the particles upon impact by ejecting powder, creating pores in some regions and compacting others. Droplet velocity in fine powders has also been shown to impact the feasibility of printing. In fine (<15 μm) 17-4 PH steel powders, balling was observed at droplet velocities of approximately 12 m/s, while parts were successfully printed at 14 m/s [34]. Droplet velocity clearly impacts BJ outcomes, but limited experimental assessment has been performed, and current models do not include its effect on printing outcomes.

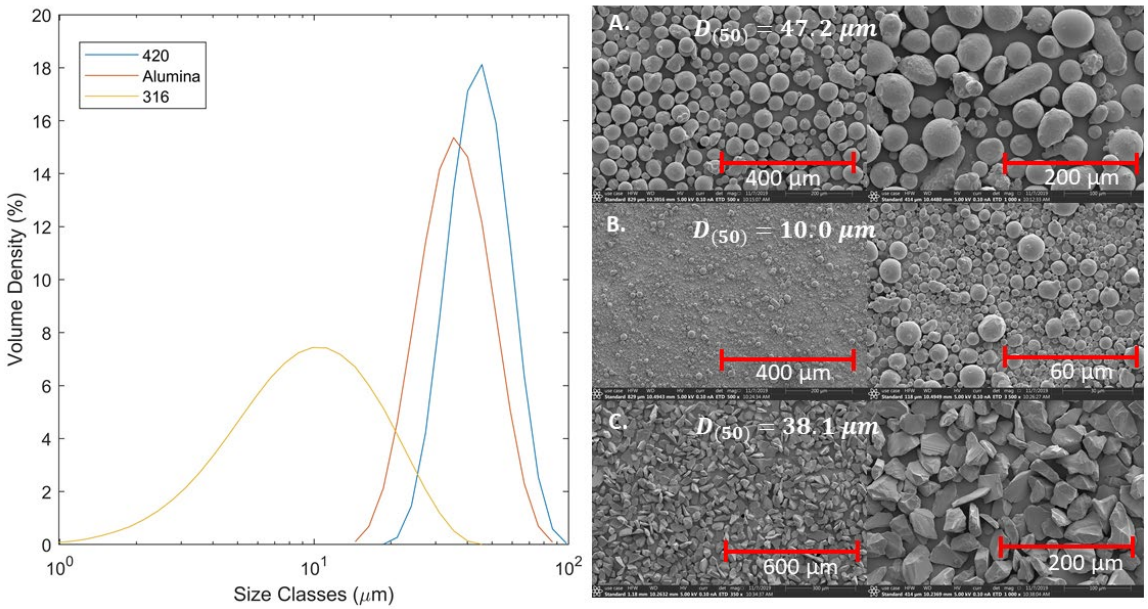

Figure 2: (Left) Particle size distribution of the test powders and (Right) SEM images of the powder morphology: A) 420 stainless steel, B) 316 stainless steel, C) Alumina.

MATERIALS

Droplet primitives and lines were printed with ExOne solvent binder with properties provided by the manufacturer (density 1.05 g/cc, viscosity 4.6 cps, surface tension 32 dynes/cm). Binder was printed into three different powders: ExOne stainless steel 420 SS, ExOne stainless steel 316 SS, and alumina abrasive 320 grit. The powders were chosen to evaluate the impact of printing parameters with powder differences. Powder size distribution was measured by NSL Analytical using laser diffraction (ISO 13320). Particle shapes were observed with images from scanning electron microscopy (Apreo C SEM). Resultant distributions and powder images are shown in Figure 2. As seen in Table 1 and Figure 2, the three powders have different particle size distributions, shapes, contact angles, packing fractions, and powder bed densities.

Table 1: Properties of powder materials used in the experiments.

	Sauter Mean Diameter, D(3,2) (μm)	Contact Angle on polished Block	Powder Bed Density (g/cm³) – Packing Fraction	Tapped Density (g/cm³)
420 Stainless Steel	45.5	33°	4.48 – 58%	4.95
316 Stainless Steel	7.58	40°	4.24 – 53%	4.64
Alumina	36.2	31°	2.01 – 51%	2.29

Contact angles of solvent binder on polished, dense samples of each material were measured using a goniometer. Rods of 420 SS and 316 SS were polished up to 1200F sand paper prior to angle

measurements. A sapphire window was used as an ideal alumina sample. Images were analyzed using ImageJ for contact angle measurements (Table 1).

METHODS

The binder/powder interactions were studied with three experimental methods (1) primitive formation from millimeter-scale droplets released from varying heights, (2) Washburn capillary rise measurement of binder/powder wetting, and (3) line printing with picoliter inkjet droplets with varied droplet velocity, spacing, and inter-arrival time.

For all tests, a uniform powder bed was created by filling shallow aluminum containers, tapping them for improved density, and leveling with an aluminum straight edge. Average density was calculated by measuring mass of the prepared powder beds and dividing by the container volume. All powder beds prepared were within ±1% packing fraction of the average reported in Table 1. Powder beds were prepared in this manner for all experiments. Washburn capillary rise used a glass tube packed to the same density as powder beds prepared with aluminum containers. Powder size, packing fraction, and powder bed density are reported in Table 1.

Millimeter-scale Droplets

Effective saturation in millimeter-scale droplets was measured by dropping millimeter-scale droplets (2-14.5 microliters) into a powder bed from varied heights (0, 10, and 20 cm; approximately 0, 1.4, and 2 m/s impact velocity respectively) as illustrated in Figure 3. ExOne solvent binder was dispensed form a micropipette at the desired heights. The powder bed was placed on a scale (Ohaus AX224, 0.1 mg resolution) to measure the mass of each droplet similar to [39]. Immediately following deposition, the powder bed was cured at 180°C for 2 hours. After curing, the primitive formed by the droplet was extracted. The mass of each droplet primitive was measured individually, and effective saturation calculated using Equation (1).

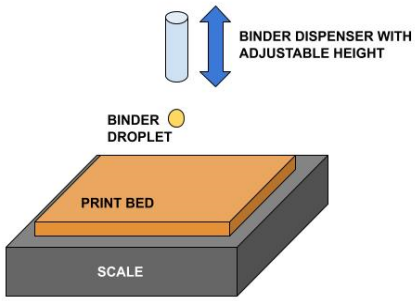

Figure 3: Illustration of the experimental procedure for millimeter-scale droplet primitives.

Washburn Capillary Rise

Washburn capillary rise method describes the wetting between binder and powder and can be used to estimate effective pore size of the powders [41-43]. In this method, a hydrophilic fabric is used to close one end of a tube. The tube is then filled with powder and tapped to increase density to the target level. The hydrophilic plug is placed on the surface of the liquid and the mass gained of

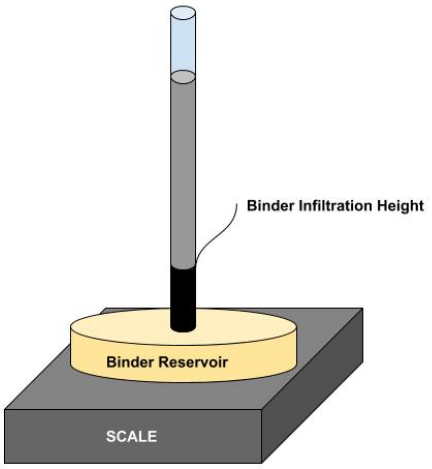

Figure 4: Left, diagram of the Washburn rise method. Right, 420 SS powder in contact with solvent binder measuring the Washburn rise.

the powder measured over time. The capillary rise has three regimes inertial, Washburn's, and late viscous. The ratio $\frac{m^2}{t}$ is constant in the Washburn regime, where m is binder mass gained and t is time in seconds. Each powder was tested three times using glass tubes 6 mm diameter and 150 mm in length. The binder absorbed over time was quantified by measuring the mass lost from the reservoir as illustrated in Figure 4.

Prior to the Washburn regime, infiltration velocity (Quéré velocity) is constant for a short period [44-46]. Early inertial regime of the capillary rise lasts just milliseconds and was unobservable with the setup. However, the Quéré velocity that characterizes this regime can be calculated. The effective pore size was estimated using the Kozeny approach using laser particle diffraction particle size measurements. The effective pore size (r_{eff}) is

$$r_{eff} = \frac{\phi\, d_{32}}{3} \frac{\epsilon}{(1-\epsilon)} \tag{2}$$

where ϵ is powder bed porosity, S_o is specific surface area of the powder, ρ_s is the density of the powder, ϕ is a shape correction factor and d_{32} is the Sauter mean diameter powder property reported in Table 1 [47]. The Sauter mean diameter is measured from laser particle diffraction. The shape correction factor is unity for spherical steel powders while the angular alumina is assumed to have cubic particles with a shape factor of 1.91. The Quéré velocity (V_q) is given by

$$V_q = \frac{2\,\gamma}{r_{eff}\,\rho_b} \tag{3}$$

where γ is the surface tension of the fluid and ρ_b is the binder density. Quéré velocity and effective pore sizes are reported in Table 2. To analyze data in the printing experiments described below, a dimensionless velocity ratio V_r was used where

$$V_r = \frac{V_d}{V_q} \tag{4}$$

and V_d is the droplet velocity.

Table 2: Powder properties of Washburn Capillary rise, effective pore size from Laser Diffraction, and Quéré velocities.

	Washburn Slope (mg^2/s)	Effective Pore Size (μm)	Quéré Velocity (m/s)
420 Stainless Steel	2.4	10.98	5.55
316 Stainless Steel	0.80	2.24	27.21
Alumina	2.1	22.03	2.77

Line Printing

A custom BJ apparatus was utilized to print lines of binder into powder with controlled droplet volume, velocity, spacing, and inter-arrival time. Each line was 20 mm in length. The apparatus consisted of a MicroFab MJ-AB-01 (40 and 30-micron orifice) print setup triggered in unison with three motorized linear stages as illustrated in Figure 5. The single nozzle print setup utilizes a pressure control system, binder reservoir, drive electronics (MicroFab Jet Drive III), and a single MicroFab print head. The pressure control maintained a vacuum on the print reservoir of -10 kPa during testing. The reservoir was maintained at the same height as the print head. Images produced from IDS UI-3370CP-M-GL camera at 2.5x magnification and a strobing LED behind the droplets were used to measure droplet velocity. The velocity was calculated by measuring the distance between droplet images from successive strobe flashes.

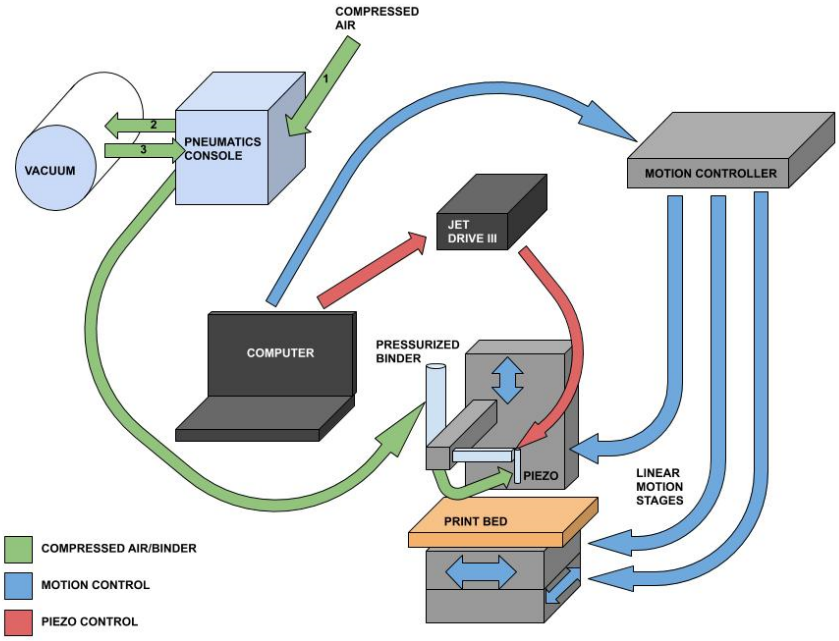

Figure 5: A diagram of the experimental apparatus and connectivity between units. The Newport linear stages controlled in unison with triggering the JetDrive III to actuate the print head and deposit lines with controlled droplet spacing. The inkjet properties (droplet velocity, droplet size) were varied using the JetDrive III waveform controls.

Line formation experiments were conducted with a range of printing parameters. From these results, a parameter map identifying conditions under which lines could be extracted for mass measurements was created for each powder for a range of droplet spacing and inter-arrival times (

Table 3) . A successful print constituted at least 50% of lines successfully extracted from the powder bed. At least 8-12 lines were printed for each condition. The various values of droplet spacing and frequency were all tested using the print head with a 30-µm orifice at a constant droplet velocity (2.6 m/s). Lines printed in 316 SS powder were analyzed before extraction using a microscope. Lines that exhibited balling were recorded and an aspect ratio of the length to width (l/w) of the ball segments were measured.

Table 3: A summary of the line experiments and parameter ranges tested for each test type.

	Powders	Droplet Velocities (m/s)	Droplet Spacing (µm)	Inter-arrival Time (ms)
Line Formation (30 µm orifice)	420 SS	2.6	5 - 15	0.4 - 2
	316 SS	2.6	2.5 - 40	0.4 - 2
	Alumina	2.6	5 - 35	0.4 - 2
Saturation (30 and 40 µm orifice)	420 SS	2.6 - 11.1	5 - 12.5	1
	316 SS	2.6 - 11.1	5 - 12.5	1
	Alumina	2.6 - 11.1	5 - 12.5	1

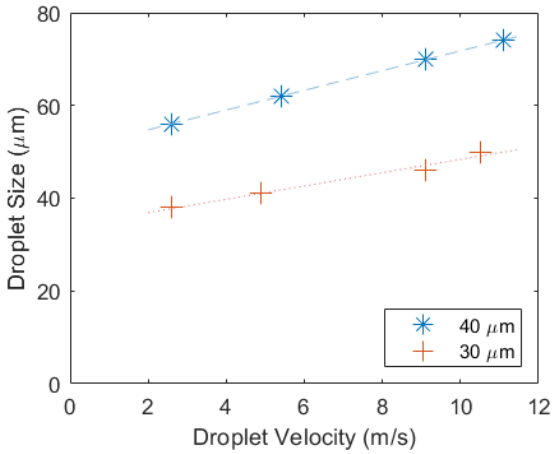

Figure 6: As droplet velocity increases the droplet size increases. The trend is linear and in both 30 and 40 μm orifice sizes.

In the line saturation studies. droplet printing frequency was maintained constant while the impact of varying saturation, droplet velocity and spacing was measured. Droplet velocity was altered by changing peak voltages sent to the print head. This also causes droplet size to change as indicated in Figure 6.

After printing, powder beds were heated in a convection oven at 180°C for 30 minutes to cure the binder. The printed lines were removed, and the mass of each line measured individually. Effective saturation of the lines was calculated using Equation (1). The mass of binder was measured by printing the equivalent of 20 lines into a container to be weighed. This method of capture included the mass of satellite droplets where present. Satellite droplets increased in volume with higher droplet velocity, but were estimated to be less than 10% of the total printed volume.

The printing parameters were summarized using dimensionless parameters. Droplet spacing was nondimensionalized as the droplet overlap ratio:

$$O_r = \frac{D_d}{l} \tag{5}$$

where D_d is the droplet diameter and l is the spacing between droplets. A mass ratio M_r was defined as:

$$M_r = \frac{M_b}{M_p} \tag{6}$$

where M_b is the mass of a single binder droplet, and M_p is the mass of an average particle size in the powder bed, assuming spherical shape at bulk density. Bond (*Bo*), Reynolds (*Re*), and Weber (W*e*) numbers are included in Table 4, calculated as follows:

$$Bo = \frac{\rho\, g\, L^2}{\gamma} \tag{7}$$

where μ is the dynamic viscosity of the binder, and L is the diameter of the droplet (Table 1).

$$Re = \frac{D_d \, V_d \, \rho_b}{\mu} \tag{8}$$

$$We = \frac{D_d \, V_d^2 \, \rho_b}{\gamma} \tag{9}$$

Table 4 summarizes the wide range of parameters tested for both the line printing and the mm-scale droplet tests.

Table 4: Parameter and property ranges in line printing experiments.

Dimensionless Parameter	Value Range
Translational Velocity	5 – 12.5 mm/s
Droplet Velocity	2.6 – 11.1 m/s
Droplet Frequency (constant)	1000 HZ
Droplet Size	38 – 74 µm
V_r (Eqn. (4)	67.4 – 558
O_r (Eqn. (5)	3.28 – 14.8
M_r (Eqn. (6)	0.089 – 53.86
Bond Number (*Bo* Eqn. (7) – Line Printing	0.0004 – 0.0018
Bond Number (*Bo* Eqn. (7) – mm Droplet	1.85 – 3.09
Reynolds Number (*Re* Eqn. (8) – Line Printing	22.6 – 187
Reynolds Number (*Re* Eqn. (8) – mm Droplet	0 – 1415
Weber Number (*We* Eqn. (9) – Line Printing	8.4 – 299
Weber Number (*We* Eqn. (9) –mm Droplet	0 – 406

RESULTS AND DISCUSSION

The experiments provided insight into the impact of printing parameters on both effective saturation levels in lines and conditions for successful line formation. These results are summarized below.

Saturation

In BJ, a target saturation value is generally selected based solely on the combination of printed binder and powder. However, a range of saturation values are possible depending on the imbibition and drainage curves because the actual effective saturation is process-dependent. In this work, the effective saturation is calculated to provide insight into the appropriate target saturation values and how they differ with printing parameters.

The average effective saturation from millimeter-scaled droplets is shown in Figure *7* as a function of droplet velocity. Over the range studied, the droplet velocity had no significant impact on the effective saturation of the droplet primitives. Alumina and 420 SS powders had similar sessile drop saturation levels, while the finer 316 SS powder had a significantly lower saturation level.

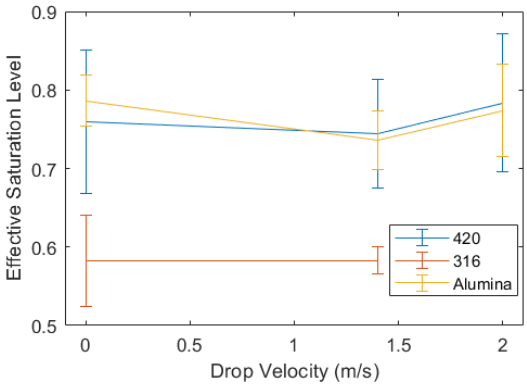

Figure 7: Millimeter-scaled droplets at various heights for equilibrium saturation calculation and comparison to line printing.

The average effective saturation of the sessile droplet (0 cm drop height, 0 m/s droplet velocity) is used as a comparison to the effective saturation of the inkjet-printed lines.

As seen in Figure 8, the lines had lower effective saturation than the sessile droplets for all powders and printing conditions. It is possible that the sessile drop saturation will provide an upper-bound for the printed saturation, but the sessile drop saturation is not an effective predictor of effective saturation in single lines. With the larger droplets from the 40 µm orifice, the effective saturation approached (but never exceeded) the sessile droplet saturation as droplet velocity decreased and overlap ratio increased.

Overlap ratio is a measure of the relative spacing of the droplets. The nondimensionalization compensates for the changing of droplet size with droplet velocity and nozzle size. Overlap ratio increases as droplet spacing decreases. Increasing overlap ratio generally causes a small increase in the effective line saturation for each orifice/material combination (Figure 8). Effective saturation is most sensitive to overlap ratio with the larger droplets (40-µm orifice) and the coarser 420 SS and alumina powders. For each droplet velocity, increasing overlap ratio increased saturation in the 420 SS and alumina powders. This suggests that the moistened powder acts to reduce the spread of the new droplets. Hapgood et. al. [48] observed that in millimeter-scale droplets, increased overlap decreased penetration time and increased saturation as well.

Both the overlap ratio and droplet velocity had a much smaller effect with the smaller droplets from the 30 µm orifice. These results suggest that the trend of BJ towards smaller droplet sizes will decrease the sensitivity of effective saturation to the printing parameters. Thus, smaller droplet sizes will allow for greater decoupling of saturation from other printing parameters.

The finer 316 SS powder has a significantly lower effective saturation for mm-scale sessile droplets than the coarser 420 SS and alumina powders. The smaller pores likely promote capillary binder infiltration compared to the larger powders—decreasing saturation. Using finer powders may also reduce the sensitivity to other printing parameters. The effective saturation of the 316 SS lines was much less sensitive to the droplet size, velocity, and overlap ratio than the coarser powders. While there is some evidence of the same trends observed in the other powders, the variation largely lies within a single standard deviation. The reduced sensitivity is a positive for

the finer 316 SS powder, but the parameter space that successfully formed a line is more limited for the 316 SS powder as shown in the line formation study.

A statistical linear regression analysis was conducted with four nondimensional numbers to evaluate the significance of four parameters (overlap ratio (O_r), velocity ratio (V_r), mass ratio (M_r), and contact angle) on the effective saturation of the lines across all printed powders and conditions. The velocity ratio, mass ratio, and contact angle each incorporate powder-specific properties (Quéré velocity, powder size/density, surface tension respectively). A p-value below 0.05 indicates that the parameter is statistically significant across all the powder data. Linear regression was done on the 40-µm orifice and 30-µm orifice separately and then on the combined dataset as reported in Table 5.

All of the printing parameters have a significant impact on effective saturation in at least one dataset as seen in Table 5. Droplet overlap ratio was statistically significant in all of the models. Significance of the overlap ratio confirms that droplets infiltrate powder differently when adjusting the amount of overlap with pre-moistened powder and/or pools of binder remaining on the surface. The velocity ratio was found significant for the combined and 40-µm datasets. The remaining parameters had variation between the different models. These results confirm that droplet spacing (overlap ratio), droplet velocity (velocity ratio) and size (mass ratio) are critical to determining the effective saturation. An understanding of how the effective saturation varies with printing parameters is particularly critical to creating fine features with high accuracy.

Table 5: Results from the nonlinear analysis. Each parameter had a coefficient and an exponent. The p-values are reported.

Orifice Size (µm)	r^2	Nondimensional Number	P-Value
40	0.78	Overlap Ratio	<0.001
		Velocity Ratio	<0.001
		Mass Ratio	0.752
		Contact Angle	0.010
30	0.47	Overlap Ratio	<0.001
		Velocity Ratio	0.429
		Mass Ratio	0.019
		Contact Angle	0.003
Combined	0.52	Overlap Ratio	<0.001
		Velocity Ratio	<0.001
		Mass Ratio	<0.001
		Contact Angle	0.143

The regression analysis reported a significantly higher r^2 value for the 40-µm orifice, 0.78, than the 30-µm orifice and combined datasets, 0.47 and 0.52 respectively. Thus, the variation in the 40-µm orifice data can be largely explained by these changing printing parameters. The lower correlation coefficients for the 30-µm orifice is partially due to the increased variation in the measurements due to the uncertainty introduced by the smaller sample masses from the smaller

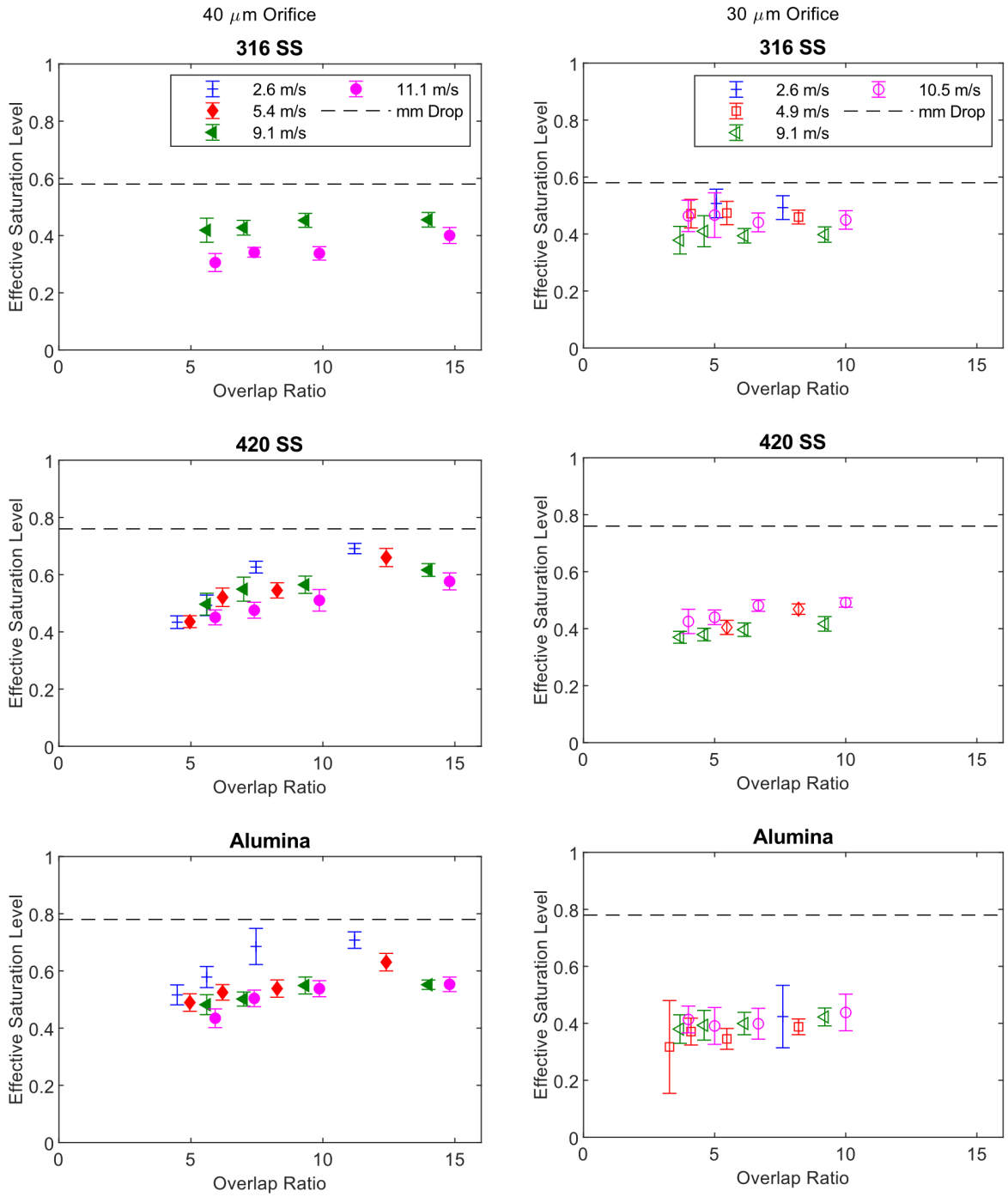

Figure 8: Plot of equilibrium saturation measured for each material (316 SS, 420 SS, Alumina) and orifice combination (40 μm orifice (left), 30 μm orifice (right)). A general trend of higher velocities and smaller overlap (larger droplet spacing) corresponds to a lower saturation levels in each of the materials with 40 μm orifice. The effective saturation of lines printed with 30 μm orifice is less sensitive to the printing parameters.

droplets produced from the 30-μm orifice. However, the smaller droplets also appear to decrease the sensitivity of the saturation to the printing parameters.

Line Formation

The success of line formation is also sensitive to printing parameters such as droplet velocity, droplet spacing, and droplet inter-arrival time. For example, at 9.1 m/s, all powders formed successful lines with both the 40- and 30-µm orifices. However, in the 316 SS, droplets from the 40-µm orifices did not coalesce to from a line when velocity was reduced to 5.4 m/s as seen in Figure 9. The inability of droplets to coalesce as a line in 316 powder with larger droplets at lower droplet velocities is evidence both of different wetting characteristics in the finer powder and for the influence of kinetic energy on line formation.

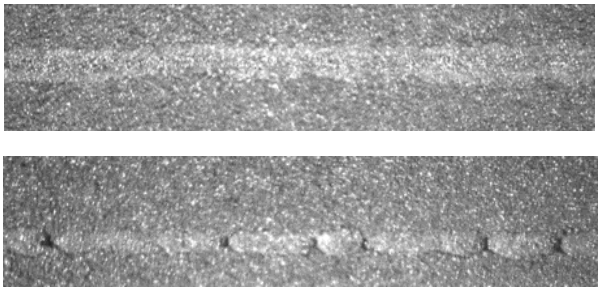

Figure 9: Lines printed in 316 SS powder (40-µm orifice). Top) 9.1 m/s droplet velocity, recoverable. Bottom) 5.4 m/s droplet velocity, unrecoverable.

Lines printed at lower velocities (5.4-2.6 m/s) with larger droplets were not included in saturation analysis in Figure 8 because they were often unrecoverable—primarily due to balling. Similar observations were found in [34], where higher droplet velocities were needed to successfully print in fine powder. Though droplet velocity did not significantly impact line saturation with smaller droplets (30-µm orifice), droplet velocity did still affect the parameter space for successful line formation. The ability to alter the droplet velocity during printing could lead to less defects in parts without altering other printing parameters such as layer thickness or saturation.

These observations led to a study of the impact of droplet spacing and droplet inter-arrival time (droplet frequency) on line formation at low droplet velocity (2.6 m/s) and small droplets (30 µm orifice) using all three powders. Sixteen lines were printed at each droplet spacing/inter-arrival time combination and then cured. For the 316 SS powder, optical imaging of the powder bed allowed clear observation of the printed features that formed from the line of droplets that were deposited. These varied in aspect ratio from 1:1 (balls) to full lines. Note that the balls are comprised of powder and binder from multiple droplets as they are over 100 µm in diameter. This provides a rich dataset that illustrates the transition from immediate balling to successful line formation.

Lines printed in 420 SS and Alumina powders could not be visually distinguished in the powder bed. To evaluate results for these materials, lines were removed from the powder bed after curing. They were lifted from below on the points of tweezers to avoid damage. Generally, nearly 100% or 0% of the lines were recovered intact, but some cases were less extreme. A minimum of 50% recovery of the printed lines was deemed successful line formation.

Figure 11 shows that the aspect ratio of the features formed when printing lines in 316 SS increases as it approaches the success/fail boundary below which lines are successfully created. Similar

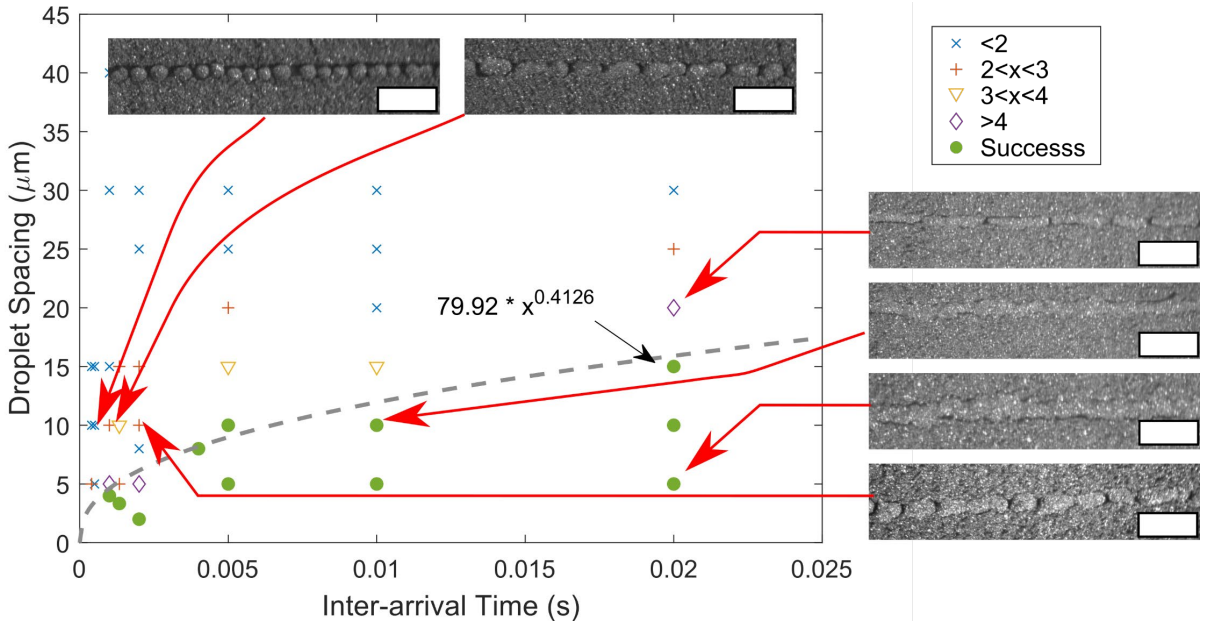

Figure 11: Initial testing of 316 SS powder to select a suitable droplet spacing and frequency. A fit to the points on the boundary between success and failure is plotted. The nonlinear relationship of the line shown is the inter-arrival time to the power of 0.4126. Unsuccessful lines are categorized by a length to width ratio of the line segments. All lines were printed at 2.6 m/s droplet velocity. Images of lines printed at corresponding print parameters are overlaid on the plot. Scale bars represent 500 μm.

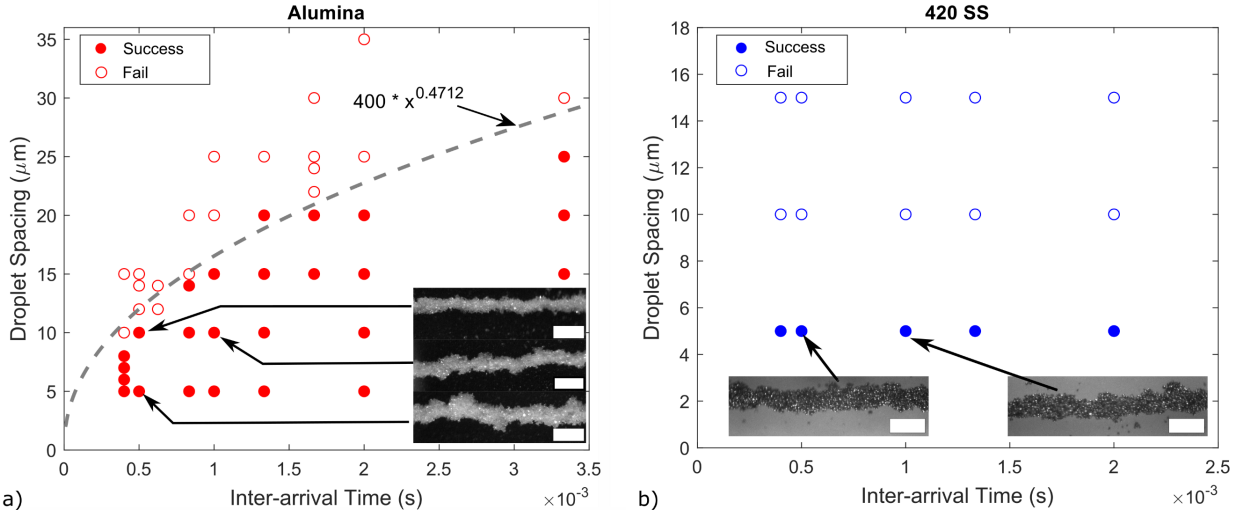

Figure 10: Success/failure regions for alumina (a) and 420 SS (b) powders. A power law fit to the data points on the success/fail boundary of the alumina produced a relationship, to the 0.4712 power, of droplet spacing and inter-arrival time. All lines printed at 2.6 m/s droplet velocity. The scale bars on the line images represents 500 μm.

transitions in from balls to lines are seen when decreasing droplet spacing and increasing droplet inter-arrival time. The formation of the lines depends on the relationship between the droplet spacing and inter-arrival time. Figure 10 plots the outcome of each line printing condition for the alumina and 420 SS as a function of droplet spacing and droplet inter-arrival time. Alumina shows a success/fail boundary similar to the 316 SS powder that depends on both droplet spacing and

inter-arrival time. However, for the same droplet spacing, the alumina can form stable lines with much shorter inter-arrival times than the 316 SS. For example, at 10 μm droplet spacing, alumina forms successful lines with 0.5 ms inter-arrival time while the minimum inter-arrival time in 316 SS was 5 ms.

Line formation success for the 420 SS (Figure 10b) appears to depend only on droplet spacing over the parameter range tested. Since droplet spacing determines the binder/length of line, this correlates with the average line diameter. Thus, these failures are likely related to line strength alone in this regime.

The line formation behavior of the 316 SS and alumina may be best explained by the imbibition characteristics. The imbibition characteristics are difficult to observe directly, but the range of droplet spacing and droplet inter-arrival times that form successful lines provides insight into the binder imbibition process. When printing a line, droplets arrive in quick succession—often faster than they absorb into the power bed. This creates an elongated pool of liquid on the surface. Observations have shown that under some circumstances, this pool will break-up into individual segments or spherical balls [31, 36, 49]. Similar challenges are observed in melt pools of powder-bed fusion processes [50]. Break-up is energetically favorable when the aspect ratio of the pool increases above a threshold level. The length of the fluid pool is related the ratio of the time for a droplet to imbibe into the powder to the printing velocity (droplet spacing/inter-arrival time) and the extent of droplet spreading. Prior work has suggested that an aspect ratio of 3.13 will cause breakup of free streams [51], but in BJ, the trailing edge of the pool is wetted into the powder bed and so the critical aspect ratio of powder is expected to deviate from the free stream value.

While the exact aspect ratio at which lines would breakup into droplets is unknown, the aspect ratio (l/w) of the pool should be related to the ratio of the line printing speed to the infiltration velocity as long as saturation is independent of the printing conditions. The saturation study showed that for the 30 μm nozzle, the variation in saturation with droplet spacing is small relative to the range of droplet spacing values and inter-arrival times studied and thus is assumed constant. Thus, the aspect ratio should be proportional to:

$$\frac{l}{w} \propto \frac{\Delta x}{\Delta t v_i} \tag{10}$$

where Δx is the droplet spacing, Δt is the droplet inter-arrival time, and v_i is the fluid infiltration velocity. Assuming that the maximum stable aspect ratio of the pool is a constant, the maximum droplet spacing for stable line formation (Δx_{max}) would be proportional to

$$\Delta x_{max} \propto \Delta t^n v_i \tag{11}$$

where the value of *n* depends on the variation of infiltration rate with time. It is expected to be 0.5 for Washburn and 1.0 for Quéré infiltration. The relationship between droplet spacing and inter-arrival time thus provides insight into the fluid infiltration velocity, how it varies with time, and the infiltration mode. To estimate this boundary, a power law curve was fit to the nearest data points on both side of the boundary of successful line formation.

Both alumina and 316 SS have exponents (n) near 0.5 with 0.4712 for alumina and 0.414 for 316 SS. The data suggest the droplets are largely absorbed in the Washburn regime. The higher Washburn slopes for the alumina compared to 316 SS (Table 2: alumina: 2.1 , 316 SS: 0.8), correlates with the ability to form lines when printing at higher droplet frequencies (shorter inter-arrival time). The smaller Washburn slopes in 316 SS may also contribute to the decreased sensitivity of the 316 SS line saturation to the printing parameters. Baker [25] previously showed an interaction between inter-arrival time and droplet spacing on the successful formation of a line with a kilohertz print head at kilohertz frequencies, but that study did not have sufficient data points to characterize the relationship.

The 420 SS has the highest Washburn infiltration rate and seemed to be insensitive to the droplet inter-arrival time. This may be because the droplets fully infiltrate faster than they can be deposited using the testing equipment. This may also relate to the larger mass of the individual powder particles of 420 SS relative to the alumina and the finer 316 SS powder. During balling, the surface tension forces may lift up powder particles that have already been wet by the binder. As the powder mass increases, this would become more difficult. Further studies with additional powder types are necessary to separate the role of particle size and density from the binder infiltration rates.

In BJ, printing speeds can be optimized by trading between droplet spacing and inter-arrival time to improve overall print quality and build rate. However, the results show that the finer 316 SS powder requires longer droplet inter-arrival time at the same droplet spacing—potentially slowing printing in the finer powders. Further study is needed to see how much this can be addressed by increasing the droplet velocity at impact or by altering the printing pattern.

This study of single lines does not represent printing of a full part, but these results are applicable to layer printing in BJ. While layer formation introduces additional factors, the layers start as a series of lines because nozzle spacing in commercial systems is significantly wider than the droplet size. Therefore, in the first phase of printing, individual lines are typically printed by each nozzle in the print head. Subsequent passes (or staggered print heads) fill in the spaces between the lines to create continuous layers. Defects such as balling could lead to large pores in the green bodies within or between layers. They may also contribute to other defects that are commonly observed in BJ parts. Line printing could also be used as a simple test to determine appropriate droplet spacing and droplet inter-arrival time.

CONCLUSION

This work studied the impact of droplet velocity, spacing, and inter-arrival time on the effective saturation of printed lines and the success of line formation. Current models disregard the kinetic energy from droplets and assume quasi-static conditions. These assumptions predict a single saturation value for all printing parameters. However, this work shows that effective saturation depends on droplet size, velocity, and spacing. As improved saturation models develop, the influence of droplet velocity and spacing should be included. The results show that lines will have less variation in saturation when using smaller droplets and smaller powder particles. Additional work is needed to study how these variables impact the formation of printed layers.

Line formation is well-studied in 2D inkjet printing on solid surfaces but has yet to be understood in BJ. This work shows that the boundary for stable line formation is influenced by the powder properties, droplet spacing, and droplet inter-arrival time. For a given powder and droplet velocity, larger droplet spacing and/or shorter inter-arrival time leads to instability in line formation. The maximum droplet spacing for successful line formation has been shown to vary with approximately the square root of the droplet inter-arrival time in the 316 SS and alumina powders which is consistent with the Washburn infiltration mode. Line formation is likely influenced by droplet velocity and droplet volume as well though these variables were not studied in this work. Line formation in the 420 SS (which had the highest Washburn infiltration slope) appeared to be independent of the droplet inter-arrival time. The reason for the difference is unknown, but this regime would be desirable to enable shorter droplet inter-arrival times which could improve printing speed.

This work demonstrates that the binder/powder interaction is complex and depends on many printing parameters that are often overlooked. Many BJ studies do not even report key printing parameters such as droplet volume, droplet velocity, printing frequency, and droplet spacing. Improved documentation of these parameters in the literature will advance understanding of the process. Increased understanding of the underlying physics will speed development of new materials and improve allocation of development resources, print quality, and process utilization in industry. However, the extension of effects seen in lines to layers and full parts is unknown and needs further study. Such studies will provide valuable insight into the impact of part geometry on the range of feasible print parameters. This understanding is critical to maximizing printing speeds, improving part accuracy, and reducing internal defects.

CRediT AUTHOR STATMENT

Trenton Colton: Investigation, Methodology, Writing-original Draft. **Nathan B. Crane:** Conceptualization, Methodology, Resources, Writing – Review & Editing, Supervision, Funding Acquisition

CONFLICT OF INTEREST

One of the authors of this paper is a member of the editorial board of this journal. To avoid potential conflict of interest, the responsibility for the editorial and peer-review process of this article lies with the journal's other editors. Furthermore, the authors of this paper were removed from the peer review process and had no, and will have no access to confidential information related to the editorial process of this article.

ACKNOWLEDGEMENTS

This work is supported in part by NSF award CMMI-1946724.

REFERENCES

[1] M. Ziaee and N. B. Crane, "Binder Jetting: A Review of Process, Materials, and Methods," *Additive Manufacturing,* 2019/06/22/ 2019, doi: https://doi.org/10.1016/j.addma.2019.05.031.

[2] X. Lv, F. Ye, L. Cheng, S. Fan, and Y. Liu, "Binder jetting of ceramics: Powders, binders, printing parameters, equipment, and post-treatment," *Ceram. Int.,* Review vol. 45, no. 10, pp. 12609-12624, 2019, doi: 10.1016/j.ceramint.2019.04.012.

[3] L. E. Murr, "Frontiers of 3D Printing/Additive Manufacturing: from Human Organs to Aircraft Fabrication†," *Journal of Materials Science & Technology,* vol. 32, no. 10, pp. 987-995, 2016/10/01/ 2016, doi: https://doi.org/10.1016/j.jmst.2016.08.011.

[4] W. Du, X. Ren, C. Ma, and Z. Pei, "Binder jetting additive manufacturing of ceramics: A literature review," in *ASME 2017 International Mechanical Engineering Congress and Exposition, IMECE 2017, November 3, 2017 - November 9, 2017*, Tampa, FL, United states, 2017, vol. 14: American Society of Mechanical Engineers (ASME), in ASME International Mechanical Engineering Congress and Exposition, Proceedings (IMECE), p. ASME, doi: 10.1115/IMECE2017-70344.

[5] B. Graybill, M. Li, D. Malawey, C. Ma, J. Alvarado Orozco, and E. Martinez Franco, *Additive Manufacturing of Nickel-Based Superalloys*. 2018, p. V001T01A015.

[6] P. Kunchala and K. Kappagantula, "3D printing high density ceramics using binder jetting with nanoparticle densifiers," *Materials & Design,* vol. 155, pp. 443-450, Oct 2018, doi: 10.1016/j.matdes.2018.06.009.

[7] T. Do, P. Kwon, and C. S. Shin, "Process development toward full-density stainless steel parts with binder jetting printing," *International Journal of Machine Tools & Manufacture,* vol. 121, pp. 50-60, Oct 2017, doi: 10.1016/j.ijmachtools.2017.04.006.

[8] E. Stevens, S. Schloder, E. Bono, D. Schmidt, and M. Chmielus, "Density variation in binder jetting 3D-printed and sintered Ti-6Al-4V," *Additive Manufacturing,* vol. 22, pp. 746-752, Aug 2018, doi: 10.1016/j.addma.2018.06.017.

[9] A. Yegyan Kumar, Y. Bai, A. Eklund, and C. B. Williams, "The effects of Hot Isostatic Pressing on parts fabricated by binder jetting additive manufacturing," *Additive Manufacturing,* vol. 24, pp. 115-124, 2018/12/01/ 2018, doi: https://doi.org/10.1016/j.addma.2018.09.021.

[10] S. M. Gaytan *et al.*, "Fabrication of barium titanate by binder jetting additive manufacturing technology," *Ceramics International,* vol. 41, no. 5, pp. 6610-19, 06/ 2015, doi: 10.1016/j.ceramint.2015.01.108.

[11] H. Miyanaji, S. Zhang, A. Lassell, A. Zandinejad, and L. Yang, "Process Development of Porcelain Ceramic Material with Binder Jetting Process for Dental Applications," *JOM,* vol. 68, no. 3, pp. 831-841, 2016/03/01 2016, doi: 10.1007/s11837-015-1771-3.

[12] J. A. Gonzalez, J. Mireles, Y. Lin, and R. B. Wicker, "Characterization of ceramic components fabricated using binder jetting additive manufacturing technology," *Ceramics International,* vol. 42, no. 9, pp. 10559-64, 07/ 2016, doi: 10.1016/j.ceramint.2016.03.079.

[13] R. K. Enneti and K. C. Prough, "Effect of binder saturation and powder layer thickness on the green strength of the binder jet 3D printing (BJ3DP) WC-12%Co powders," *International Journal of Refractory Metals and Hard Materials,* vol. 84, p. 104991, 2019/11/01/ 2019, doi: https://doi.org/10.1016/j.ijrmhm.2019.104991.

[14] M. T. Stawovy, K. Myers, and S. Ohm, "Binder jet printing of tungsten heavy alloy," *International Journal of Refractory Metals and Hard Materials,* vol. 83, p. 104981, 2019/09/01/ 2019, doi: https://doi.org/10.1016/j.ijrmhm.2019.104981.

[15] N. B. Crane, "Impact of part thickness and drying conditions on saturation limits in binder jet additive manufacturing," *Additive Manufacturing,* vol. 33, p. 101127, 2020/05/01/ 2020, doi: https://doi.org/10.1016/j.addma.2020.101127.

[16] X. D. Cheng, Y. L. Zhu, L. Zhang, D. Y. Zhang, and T. Ku, "Numerical analysis of deposition frequency for successive droplets coalescence dynamics," *Physics of Fluids,* vol. 30, no. 4, Apr 2018, Art no. 042102, doi: 10.1063/1.5022511.

[17] D. Soltman and V. Subramanian, "Inkjet-Printed Line Morphologies and Temperature Control of the Coffee Ring Effect," *Langmuir,* vol. 24, no. 5, pp. 2224-2231, 2008/03/01 2008, doi: 10.1021/la7026847.

[18] Z. Du, R. Xing, X. Cao, X. Yu, and Y. Han, "Symmetric and uniform coalescence of ink-jetting printed polyfluorene ink drops by controlling the droplet spacing distance and ink surface tension/viscosity ratio," *Polymer,* vol. 115, pp. 45-51, 2017, doi: 10.1016/j.polymer.2017.03.023.

[19] H. Miyanaji, N. Momenzadeh, and L. Yang, "Effect of printing speed on quality of printed parts in Binder Jetting Process," *Additive Manufacturing,* Article vol. 20, pp. 1-10, 2018, doi: 10.1016/j.addma.2017.12.008.

[20] N. D. Parab *et al.*, "Real time observation of binder jetting printing process using high-speed X-ray imaging," *Scientific Reports,* vol. 9, no. 1, p. 2499, 2019/02/21 2019, doi: 10.1038/s41598-019-38862-7.

[21] Y. Bai, G. Wagner, and C. B. Williams, "Effect of Particle Size Distribution on Powder Packing and Sintering in Binder Jetting Additive Manufacturing of Metals," (in English), *J. Manuf. Sci. Eng.-Trans. ASME,* Article vol. 139, no. 8, p. 6, Aug 2017, Art no. 081019, doi: 10.1115/1.4036640.

[22] M. Vaezi and C. K. Chua, "Effects of layer thickness and binder saturation level parameters on 3D printing process," (in English), *International Journal of Advanced Manufacturing Technology,* Article vol. 53, no. 1-4, pp. 275-284, 2011, doi: 10.1007/s00170-010-2821-1.

[23] W.-K. Hsiao, G. D. Martin, and I. M. Hutchings, "Printing Stable Liquid Tracks on a Surface with Finite Receding Contact Angle," *Langmuir,* vol. 30, no. 41, pp. 12447-12455, 2014/10/21 2014, doi: 10.1021/la502490p.

[24] P. C. Duineveld, "The stability of ink-jet printed lines of liquid with zero receding contact angle on a homogeneous substrate," *Journal of Fluid Mechanics,* vol. 477, pp. 175-200, 2003, doi: 10.1017/S0022112002003117.

[25] P. R. Baker, "Three dimensional printing with fine metal powders," Massachusetts Institute of Technology, 1997.

[26] K. Lu and W. T. Reynolds, "3DP process for fine mesh structure printing," *Powder Technology,* vol. 187, no. 1, pp. 11-18, 2008, doi: 10.1016/j.powtec.2007.12.017.

[27] H. Tan, "Three-dimensional simulation of micrometer-sized droplet impact and penetration into the powder bed," *Chemical Engineering Science,* vol. 153, pp. 93-107, 2016, doi: 10.1016/j.ces.2016.07.015.

[28] H. Miyanaji, S. Zhang, and L. Yang, "A new physics-based model for equilibrium saturation determination in binder jetting additive manufacturing process," *International Journal of Machine Tools and Manufacture,* vol. 124, pp. 1-11, 2018, doi: 10.1016/j.ijmachtools.2017.09.001.
[29] J. Bear, *Modeling phenomena of flow and transport in porous media*. Springer, 2018.
[30] Y. Bai, C. Wall, H. Pham, A. Esker, and C. B. Williams, "Characterizing Binder-Powder Interaction in Binder Jetting Additive Manufacturing Via Sessile Drop Goniometry," *J. Manuf. Sci. Eng.-Trans. ASME,* vol. 141, no. 1, Jan 2019, Art no. 011005, doi: 10.1115/1.4041624.
[31] J. Bredt, "Binder Stability and Powder/Binder Interaction in Three Dimensional Printing," *MIT Thesis,* 1995.
[32] T. Colton, J. Liechty, A. McLean, and N. B. Crane, "Influence of Drop Velocity and Droplet Spacing on the Equilibrium Saturation Level in Binder Jetting," *Solid Freeform Fabrication 2019: Proceedings of the 30th Annual International Solid Freeform Fabrication Symposium — An Additive Manufacturing Conference,* p. 9, 2019 2019.
[33] T. Nguyen, W. Shen, and K. Hapgood, "Drop penetration time in heterogeneous powder beds," *Chemical Engineering Science,* Article vol. 64, no. 24, pp. 5210-5221, 2009, doi: 10.1016/j.ces.2009.08.038.
[34] K. J. Seluga, "Three Dimensional Printing by Vector Printing of Fine Metal Powders," *Department of Mechanical Engineering, MIT,* 2001.
[35] W.-K. Hsiao and E. S. Betton, "Coalescence and Line Formation," in *Fundamentals of Inkjet Printing*, pp. 219-250.
[36] T. Fan, "Droplet-powder impact interaction in three dimentional printing," *MIT Thesis,* Thesis 1996.
[37] H. N. Emady, D. Kayrak-Talay, and J. D. Litster, "A regime map for granule formation by drop impact on powder beds," *AIChE Journal,* Article vol. 59, no. 1, pp. 96-107, 2013, doi: 10.1002/aic.13952.
[38] H. N. Emady, D. Kayrak-Talay, W. C. Schwerin, and J. D. Litster, "Granule formation mechanisms and morphology from single drop impact on powder beds," *Powder Technology,* vol. 212, no. 1, pp. 69-79, 2011, doi: 10.1016/j.powtec.2011.04.030.
[39] T. Gao *et al.*, "Granule formation and structure from single drop impact on heterogeneous powder beds," *International Journal of Pharmaceutics,* Article vol. 552, no. 1-2, pp. 56-66, 2018, doi: 10.1016/j.ijpharm.2018.09.036.
[40] J. O. Marston, J. E. Sprittles, Y. Zhu, E. Q. Li, I. U. Vakarelski, and S. T. Thoroddsen, "Drop spreading and penetration into pre-wetted powders," *Powder Technology,* vol. 239, pp. 128-36, 2013, doi: 10.1016/j.powtec.2013.01.062.
[41] A. Alghunaim, S. Kirdponpattara, and B.-m. Z. Newby, "Techniques for determining contact angle and wettability of powders," *Powder Technology,* vol. 287, pp. 201-215, 2016/01/01/ 2016, doi: https://doi.org/10.1016/j.powtec.2015.10.002.
[42] L. L. Popovich, D. L. Feke, and I. Manas-Zloczower, "Influence of physical and interfacial characteristics on the wetting and spreading of fluids on powders," *Powder Technology,* vol. 104, no. 1, pp. 68-74, 1999/08/03/ 1999, doi: https://doi.org/10.1016/S0032-5910(99)00030-3.

[43] E. W. Washburn, "The Dynamics of Capillary Flow," *Physical Review,* vol. 17, no. 3, pp. 273-283, 03/01/ 1921, doi: 10.1103/PhysRev.17.273.
[44] D. Quéré, "Inertial capillarity," *Europhysics Letters,* Article vol. 39, no. 5, pp. 533-538, 1997, doi: 10.1209/epl/i1997-00389-2.
[45] A. Siebold, M. Nardin, J. Schultz, A. Walliser, and M. Oppliger, "Effect of dynamic contact angle on capillary rise phenomena," *Colloids and Surfaces A: Physicochemical and Engineering Aspects,* vol. 161, no. 1, pp. 81-87, 2000/01/15/ 2000, doi: https://doi.org/10.1016/S0927-7757(99)00327-1.
[46] N. Fries and M. Dreyer, "The transition from inertial to viscous flow in capillary rise," *Journal of Colloid and Interface Science,* vol. 327, no. 1, pp. 125-128, 2008/11/01/ 2008, doi: https://doi.org/10.1016/j.jcis.2008.08.018.
[47] K. P. Hapgood, J. D. Litster, S. R. Biggs, and T. Howes, "Drop Penetration into Porous Powder Beds," *Journal of Colloid and Interface Science,* vol. 253, no. 2, pp. 353-366, 2002/09/15/ 2002, doi: https://doi.org/10.1006/jcis.2002.8527.
[48] K. P. Hapgood, T. H. Nguyen, S. Hauw, S. M. Iveson, and W. Shen, "Rewetting effects and droplet motion on partially wetted powder surfaces," *AIChE Journal,* Article vol. 55, no. 6, pp. 1402-1415, 2009, doi: 10.1002/aic.11772.
[49] M. Lanzetta and E. Sachs, "Improved surface finish in 3D printing using bimodal powder distribution," *Rapid Prototyping Journal,* vol. 9, no. 3, pp. 157-66, 2003, doi: 10.1108/13552540310477463.
[50] J. P. Kruth, G. Levy, F. Klocke, and T. H. C. Childs, "Consolidation phenomena in laser and powder-bed based layered manufacturing," *CIRP Annals,* vol. 56, no. 2, pp. 730-759, 2007/01/01/ 2007, doi: https://doi.org/10.1016/j.cirp.2007.10.004.
[51] J. Plateau, *Experimental and theoretical statics of liquids subject to molecular forces only*, *Gauthier-Villars, Paris,* vol. 4, 1873.